Numerical investigation of concrete-filled steel tubular tied arch bridge under travelling vehicles

Jianrong Yang
Faculty of Civil Engineering and Architecture, Kunming University of Science and Technology, Kunming, China

Jianzhong Li
Department of Bridge Engineering, Tongji University, Shanghai, China

Junxin Shen
Broadvision Engineering Consultants, Kunming, China

ABSTRACT: A theoretical research in relation to the dynamic impact effects of concrete-filled steel tubular (CFST) tied arch bridge under travelling vehicles was described. The equations of the coupled system were derived based on Modal Coupled Method and solved with Wilson-θ method. The mathematical model assumed a three dimensional finite element representation of the bridge together with beam, shell, and link elements. And the vehicle simulation employed a 3D linear vehicle model with seven degrees of freedom. A well-known power spectral density of road pavement profiles defined the deck surface roughness for Perfect, Good, and Poor roads respectively. In this way, the dynamic interaction between the bridge and vehicle model was simulated. And the dynamic amplification factors (DAF) were computed for displacement and internal force respectively. The impact effects of the vehicle on different bridge members and influence factors were studied. Meanwhile, the acceleration responses of some components were analyzed in the frequency domain. Some valuable conclusions have been drawn from the results.

1 INTRODUCTION

With the development of new technology and methods of analysis, more sophisticated models of vehicle and bridge were employed to investigate the vehicle-bridge interaction problem. Based on these more realistic models, dynamic equilibrium equation of vehicle-bridge system is set up and solved by numerical integration. This makes it possible for researchers to study the influence of different factors on the dynamic behaviour of bridges, such as road surface profile, braking, inelastic suspension system of vehicles etc.

Most of the recent studies focus mainly on beam type bridges, and comparatively few works deal with the other types of bridges. Among them plan frame element is usually applied to build bridge models. But analytical models like this make too many simplifications to provide accurately the dynamic characteristics of the structures especially those whose vibration is governed by more than one mode (e.g. arch bridge, cable stayed bridge, curved and skew bridge).

Inspired by a series of accidents of structural failure (Lu 2005), the dynamic behaviour of tied-arch bridge due to heavy vehicle loads has become an interesting subject since recently. CFST tied-arch bridge is more competitive than the other tied-arch bridges in china for their lower building cost, convenience of constructing, and lower demands on soil foundation. However the design theory of this type of bridge has been left far behind their engineering practice. After decades of operation some of them are subject to damages induced by traffic loads. Different researchers have committed themselves to the investigation of vehicle induced vibration of CFST tied-arch bridge and obtained some valuable results. Wu et al. studied the bridge-vehicle dynamics characteristic of Nielsen arch bridge in high speed railway. In their research the difference between the X style arch and the parallel arch in bridge was compared.

Shan et al. evaluated the vertical and transverse displacements of X style arch bridge, its dynamic amplification factor, and the offload factors of vehicles. Roeder conducted an on-the-spot experiment research on a steel tied-arch bridge, and the measured DAF varied between 0.9-1.7 for the floor beams, 0.6-1.1 for the stringers, 0.94-1.35 for arch rib and hanger were reported respectively. Li et al. carried out an model test on Nielsen X style CFST tied-arch bridge, and force distribution and loading resisting capacity of this type of structure was thoroughly studied. Field testing and simulation of a tied-arch bridge was performed by Malm to study the fatigue in various structural components according Palmgren-Miner's rule. The measured data results were compared with those from the FE model to give a better understanding of the dynamic behaviour of the bridge.

The primary objective of this study is to investigate numerically vehicle induced vibration of CFST tied-arch bridge. Based on Modal Coupled Method, the equations of motion of coupled road vehicle-bridge system are established and solved by Wilson-θ method. A comprehensive computer program is accordingly developed. Dynamic responses of the bridge, such as displacement, internal force, and acceleration are computed and discussed in detail. The results obtained provide a background for verification and modification of highway bridge design and evaluation specifications.

2 VEHICLE AND BRIDGE MODEL

2.1 Bridge model

In order to obtain representative results, the general structural arrangement was determined according to the design of similar bridges (Chen 2002). The bridge is a through tied-arch bridge with CFST arch ribs. It is 90 m long and 20.7 m wide, with 13 bays in the arch and floor system. The arch ribs are shaped into catenaries m=1.1, rise-span ratios =1/5, and connected by 5 braces. The depth of the main arch rib is 2300 mm. The cross-section of the two main arch ribs comprises dumbbell-type concrete-filled steel tubes with the dimensions of 900×14 mm and C50 expansive concrete filled. There are 12 hangers made of 109ϕ7 high strength steel wire on each side of the bridge. They are numbered from 1 to 12 where hanger 1 and 12 are the shortest and hanger 6 is the longest. The main arch ribs are connected individually by eight pre-stressed strands on each side in the longitudinal direction, which act as tie bars and was pre-stressed by 11200 kN force. The floor system consists of a 330 mm thick concrete slab supported directly by cross girders at a spacing of 6.9 m.

A three dimensional finite element model (FEM) was developed for the bridge in the general commercial FE package ANSYS as shown in Fig.1. The arch ribs are composed of steel tube and concrete which is supposed to work together. Therefore the steel tube and its filled-in concrete were represented separately as two-node beam elements (BEAM44) which share the same group of nodes. The beams (both transverse and longitudinal), hangers, and braces were modelled as beam elements (Beam44). The deck slab was modelled using shell elements (SHELL43). The two supports of each rib were connected horizontally by link elements (LINK8) to model the tie chords.

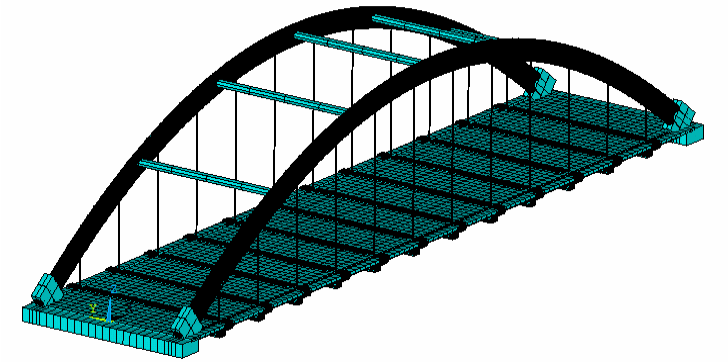

Figure 1 : Finite element model of the bridge

A total of 300 modes are computed by subspace iteration method. The first vibration mode is symmetric transverse bending of the main arches with a frequency of 0.4610 Hz. This matches the common feature that, for CFST tied-arch bridges, the in-plane stiffness of the arch ribs is superior to that of out-of-plane. The second mode is vertical antisymmetric bending in 0.9447 Hz. The hangers have higher natural frequencies in the longitudinal direction due to the higher degree of restraint in the connection with the main arches and transverse beams. Since the hangers have different lengths and axial pre-stress, their natural frequencies differ from each other between 6.1395 and 19.4649 Hz.

2.2 Vehicle model

As shown in Fig.2, the vehicle model is composed of one vehicle body and four wheel bodies. The tires and suspension systems are idealized as linear elastic spring elements and dashpots. The vehicle body has three degrees of freedom, including z displacement, rolling, and pitching; each wheel has only one degree of freedom, namely z displacement. Therefore, each vehicle has a total of seven degrees of freedom.

Here, the mass of vehicle body m_s=2.55E4 kg; the pitching (J_θ) and rolling (J_α) moment of inertia of vehicle body are 5.53E4 kg·m^2/rad and 56.89E3 kg·m^2/rad respectively; the damping coefficients of vehicle suspension (c_{s1}, c_{s2}, c_{s3}, c_{s4}) are 2.00E4 N·s/m; the spring stiffness coefficient of vehicle suspension for the front (k_{s1}, k_{s2}) and rear (k_{s3}, k_{s4}) axles are 4.00E6 and 8.00E6 N/m respectively; the mass of each front axle tires are 445 kg; the mass of each rear axle tires are 890 kg; the damping coefficient for each tires (c_{t1}, c_{t2}, c_{t3}, c_{t4}) is 2.00E4 N·s/m; the spring stiffness coefficient of tires for the front (k_{t1}, k_{t2}) and rear (k_{t3}, k_{t4}) axles are 2.25E6 and 8.00E6 N/m respectively; distance α_1, α_2, b_1, and b_2 are 3.479, 1.021, 0.915, 0.915 m respectively (Fafard, Laflamme, Savard and Bennur 1998). The seven frequencies of the vehicle are calculated as 2.03, 3.22, 4.27, 18.91, 19.77, 21.41 and 21.63 Hz respectively with Stodola method (Bhatt, 2002).

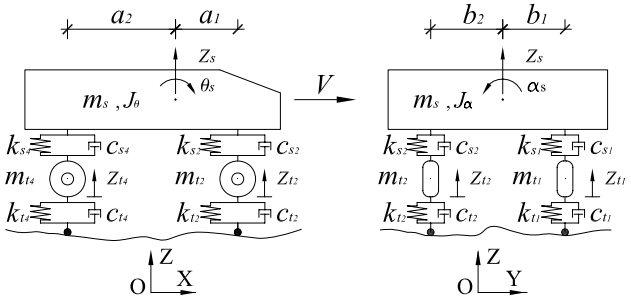

Figure 2 : Three dimensional vehicle model of seven degree of freedom

3 VEHICLE-BRIDGE DYNAMIC SYSTEM

3.1 Vehicle-bridge model

The modal equations of a bridge can be expressed as

$$[M_B]\{\ddot{A}\}+[C_B]\{\dot{A}\}+[K_B]\{A\}=\{F_B\} \tag{1}$$

where $\{A\}$=modal displacement vector; $[M_b]$=modal mass matrix; $[C_b]$=modal damping matrix; and $[K_b]$=modal stiffness matrix of the bridge; $\{F_b\}$=modal wheel-bridge contact force vector on the bridge. The equations of motion for the vehicle model presented in Figure 2 are Lagrange's formulation as

$$[M_V]\{\ddot{Z}\}+[C_V]\{\dot{Z}\}+[K_V]\{Z\}=\{F_V\} \tag{2}$$

where $\{F_V\}$ is the contact force vector applied on the vehicle; $[M_V]$, $[C_V]$ and $[K_V]$ are, respectively, the mass, damping and stiffness matrices of the vehicle. And $\{Z\}$ is the vertical displacement vector of the vehicle degrees of freedom.

3.2 Interaction of vehicle and bridge

The interaction force between the bridge and the vehicle on ith wheel is given by

$$F_{ti} = -k_{ti}(Z_{ti} - U_{bi} - r_i) - c_{ti}(\dot{Z}_{ti} - \dot{U}_{bi} - U'_{bi}V - r'_iV) \tag{3}$$

k_{ti} and c_{ti} are, respectively, the tire stiffness and tire damping of the ith wheel; Z_{ti} is the vertical displacement of the ith wheel; U_{bi} and r_i are, respectively, the bridge vertical displacement and the road surface roughness under the ith wheel; and V is the speed of the vehicle. Based on the jth modal displacement under the ith wheel ϕ_j^i, U_{bi} can be expressed with modal linear superposition technique as

$$U_{bi} = \sum_{j=1}^{N} \phi_j^i A_j \tag{4}$$

where N=dimension of the modal space. The force acted on bridge deck by ith wheel is expressed as $F_{bi}=F_{Gi}-F_{ti}$, in which F_{Gi} is the vehicle gravity under the ith wheel. While the nth to mth wheel of the vehicle is located on the deck, the Lth modal force in Eq. (1) can be derived as

$$F_{BL} = \sum_{i=n}^{m} \phi_L^i F_{bi} \tag{5}$$

Substituting Eq. (5) into Eq. (1) for all modes, then it becomes

$$\begin{bmatrix} [M_V] & [0] \\ [0] & [M_B] \end{bmatrix} \begin{Bmatrix} \{\ddot{Z}_v\} \\ \ddot{A} \end{Bmatrix} + \begin{bmatrix} [C_V] & [C_{Bt}] \\ [C_{Bt}]^T & [C_B + C_{BV}] \end{bmatrix} \begin{Bmatrix} \{\dot{Z}_V\} \\ \{\dot{A}\} \end{Bmatrix} + \begin{bmatrix} [K_V] & [K_{Bt1}] \\ [K_{Bt2}] & [K_B + K_{BV}] \end{bmatrix} \begin{Bmatrix} \{Z_V\} \\ \{A\} \end{Bmatrix} = \{F\} \tag{6}$$

where the additional terms C_{Bt}, C_{BV}, K_{Bt1}, K_{Bt2}, K_{BV} are due to the contact force. They are all functions of bridge properties, vehicle properties and the positions of vehicle-bridge contact points. This indicates that the additional terms in Eq. (6) are time-dependent terms and will change as the vehicle moves across the bridge.

3.3 Road surface profile

A vehicle travelling over a bridge and its approach roadways which containing surface irregularities experiences vertical and horizontal motions. These motions create additional forces in addition to the vehicle load. They depend on the suspension characteristics, condition of the pavement, and speed of the vehicle. The typical road surface may be described by a periodically modulated random process. One method of characterizing a random function is by use of the power spectral density (PSD) function. Dodds and Robson have developed a typical PSD function that can be approximated by an exponential function as

$$S(f) = \begin{cases} S(f_0)(f/f_0)^{-a_1}, & f \le f_0 \\ S(f_0)(f/f_0)^{-a_2}, & f \ge f_0 \end{cases} \tag{7}$$

where $S(f)$=PSD function (m^2/*cycle*/*m*) for the road surface elevation; f=wave number (cycle/m); f_0=the discontinuity frequency (cycle/m, $1/2\pi$); the values of α_1, α_2 are taken as 2 and 1.4; $S(f_0)$ =roughness coefficient (m^2/*cycle*/*m*), and its value is chosen depending on the road condition.

The road surface profile modelled as a stationary Gaussian random process can be generated by an inverse Fourier Transform as follows:

$$R(x) = \sqrt{2}\sum_{k=1}^{N}\sqrt{S(f_k)\Delta f}\cos(2\pi f_k x + \theta_k) \tag{8}$$

where $R(x)$=road surface profile (m); $S(f_k)$=PSD function ($m^2/cycle/m$); f_k=wave number/spatial frequency ($cycle/m$); Δf=the sampling bandwidth of spatial frequency ($cycle/m$); θ_k=the random number uniformly distributed in [0, 2π]; N=number of sampling frequencies. In this paper, the values of 0, 16, 256 (10^{-6} $m^2/cycle/m$) are used according to International Standard Organization (ISO) specifications (ISO 1995), as the roughness coefficients for the class of Perfect, Good, and Poor roads respectively. The generated sample road surface profile with road roughness is shown in Fig.3.

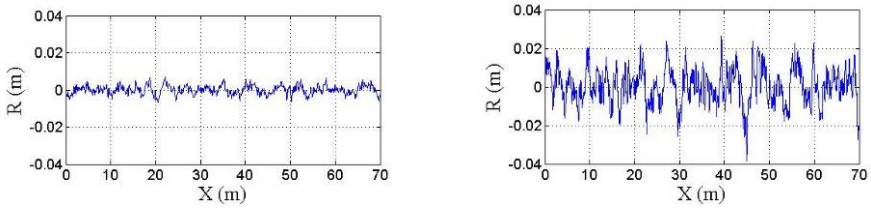

(a) (b)

Figure 3 : Road surface profile with road roughness: (a) Road surface profile, Good (b) Road surface profile: Poor

In the present study, the random road surface profiles were generated once and then used for all calculations. This approach excludes the uncertainty of surface profiles (because each run could generate a different profile) for the comparison study.

4 NUMERICAL RESULTS

As the dynamic characteristics of the system are obtained, the vehicle-bridge interaction process is simulated with Modal Coupled Method. Modal damping ratio of each mode is taken as constant deliberately ξ=0.03. Initially, both the vehicle and bridge are assumed to be at rest and the vehicle is traveling forward at a uniform speed. The vehicle was modeled with a 20 m lead distance to minimize the effect of initial conditions on bridge vibration. The same class of road surface is assumed for both the approach roadway and bridge decks. And road surface profile remains fixed alone the transverse direction. Three vehicle trajectories, namely TR1, TR2, and TR3, are considered in order to determine the maximum traffic action effects. They are all parallel to the center line of the bridge and drift off the line by 0, 3.6, and 7.2 m respectively. Vehicle speeds ranging from 10 to 40 m/s are considered which cover the speed limit of most highways. The time steps chosen were relatively short in order to scan the road surface profile correctly and to avoid convergence problems. In all runs, the vehicle progressed over the bridge in steps of 0.005 m. Therefore each simulation required 22 900 steps.

The vehicle dynamic amplification factor (DAF) is expressed as the ratio of maximum dynamic response R_D to maximum static response R_S: DAF=R_D/R_S. In this study DAFs were calculated for vertical displacement, bending moment, and axial force respectively.

4.1 Vertical displacement

Dynamic displacements in vertical direction are computed for the arch ribs, slaps, and hangers respectively. The displacement value U_Z is measured upwards from the original position of structure if U_Z is positive or downwards if U_Z is negative. The typical displacement time histories of middle span slab at a speed of 20 m/s are shown in Fig.4. The simulations were

carried out for three different road surface profiles with the vehicle passing along different trajectories. The figure shows that the dynamic response curves fluctuate near the corresponding influence lines, considering the effects of vehicle mass, speed, road surface profile, and trajectory. The highest displacements occur for the Poor road surface profile. At each data point, the extreme dynamic and static displacements correspond to the same critical trajectory. For the data points of arch ribs the critical trajectory may be TR1, and TR3; for the points of the hangers, it is TR3 that matters. It can be seen from the figure that the worse the bridge road condition, the larger the bridge dynamic displacement under the truck load. The displacements are small because the truck is relatively light. The same law applies to the other components as well.

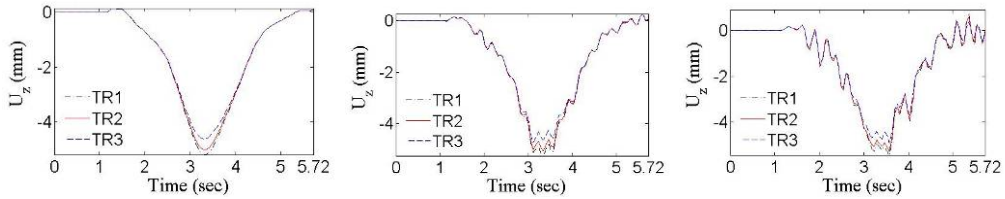

Figure 4 : Vertical displacement of middle span slab (V=20 m/s): (a) Perfect road (b) Good road (c) Poor road

In accordance with the definition of DAF, the dynamic displacements of middle span slab and corresponding DAFs under different vehicle speeds and road surface profiles are listed out in Table 1. If the displacement DAF of middle span slab is regarded as the global DAF for the whole bridge, its value is closely related to road surface profile. Usually surface profiles of most highways can be classified as Good, then the DAFs calculated vary between 1.02 and 1.11.

Table 1 : Maximum displacement and DAFs of middle span slab

Profile	Speed	Ud	DAF	Speed	Ud	DAF
	m/s	mm		m/s	mm	
Perfect	10	-7.15	1.00	30	-7.28	1.02
Good	10	-7.40	1.04	30	-7.27	1.02
Poor	10	-7.49	1.05	30	-8.62	1.21
Perfect	20	-7.20	1.01	40	-7.90	1.11
Good	20	-7.33	1.03	40	-7.92	1.11
Poor	20	-7.51	1.05	40	-9.72	1.36

The DAFs specified in various codes for the bridge are summarized in Table 4. It is noted that the DAF specified in China code (2004) is much lower than those in the other codes (OHBDC 1983, AASHTO 2005, AASHTO 2002) and many of the values in Table 1. When the road surface profile is Poor, the DAFs calculated vary between 1.05 and 1.36 which exceed the DAFs specified in the design codes by a large margin.

Table 2 : DAFs in various codes

Code	DAF
China Code JTG D60-2004	1.05
OHBDC	1.20
AASHTO LRFD	1.15（Fatigue and fracture limit state）
	1.33（All other limit states）
AASHTO Standard Specifications	1.12

4.2 Internal force

Traditionally DAFs defined in codes have classically been derived from global traffic action effects in the main structural elements of bridges, e.g. middle span slabs. And they are applied to the design of the whole bridge. However local dynamic effects in different components of the structure may be quite different. Furthermore DAFs of the same component, but derived from different action effects, may still be greatly different from each other. It is necessary to calculate accurately the DAFs of internal force for individual component.

Table 3 summarizes the DAFs of the arch ribs and hangers on three key sections. The truck passed over the bridge with speeds that vary from 10 to 40 m/s and Good road surface profile. The effects including axial force N, bending moment M, and stress amplitude $\Delta\sigma$ were applied to calculate the DAFs. Compared to Table 1, it is known that local DAFs on the key sections all exceed the global ones.

DAFs of the arch ribs derived from axial force differ significantly from those from bending moment with extreme discrepancy of 31% in middle span; DAFs of the hangers derived from axial force and stress amplitude respectively are also considerably different with extreme discrepancy of 13% in 3/4 span. Therefore it appears to be unreasonable to take into account the dynamic effect of traffic actions using a single global DAF. Moreover local DAF should be chosen carefully according to the type of components and the action effects to be considered. Also the calculated local DAFs exceed the global one specified in China code by a large margin, but meet the requirement of AASHTO code. When the road surface profile is Poor, the local DAFs calculated increase at different extent depending on the type of components and the effects.

Table 3 : DAFs of the arch and hanger on the key sections

Component	Location	1/4 span		Middle span		3/4 span	
Arch rib	Effect	N	M	N	M	N	M
	Positive value	-	1.27	-	1.51	-	1.31
	Negative value	1.24	1.19	1.15	1.19	1.13	1.35
Hanger	Effect	N	$\Delta\sigma$	N	$\Delta\sigma$	N	$\Delta\sigma$
	Positive value	1.13	1.23	1.05	1.14	1.15	1.30

4.3 Acceleration response in frequency domain

After its acceleration time histories are transformed from time domain to frequency domain by fast Fourier transform (FFT), the performance of the bridge can also be clearly observed for the accelerations in the frequency domain. The time history and function of power spectral density (PSD) for the arch rib and slab in middle span are shown in Fig.5.

The curves in time domain are quite different, but they have similar characteristics in frequency domain. For the arch rib the peaks can be observed in frequencies of 0.8666 and 3.2932-3.4647 Hz respectively which are close to the 2nd, 10th and 11th vibration modes of the bridge. As to the slab the peaks fall into frequencies of 0.8666 and 4.1590-4.3329 Hz respectively which are close to the 2nd and 13th modes. Both the arch rib and slab respond strongly in a frequency of 0.8666 Hz which is close, but not equal, to 0.9447 Hz (the second mode of the bridge) because of the influence of vehicle mass. When road surface profile is considered, some of the higher modes will be excited due to the intensified vibration of the vehicle.

Though the hangers have different dynamic characteristics, they vibrate primarily with the first natural frequency. The peaks on the PSD curve are distributed in the frequency range of 18.1982-19.9325 Hz, 8.1459-8.4926 Hz, and 4.1596-6.2394 Hz respectively for side hangers, 1/4 span hangers, and middle span hangers. Along the PSD curves of longitudinal acceleration, the peaks are observed at low frequencies. The reason for this is that the hangers vibrate simultaneously by itself and together with the whole bridge.

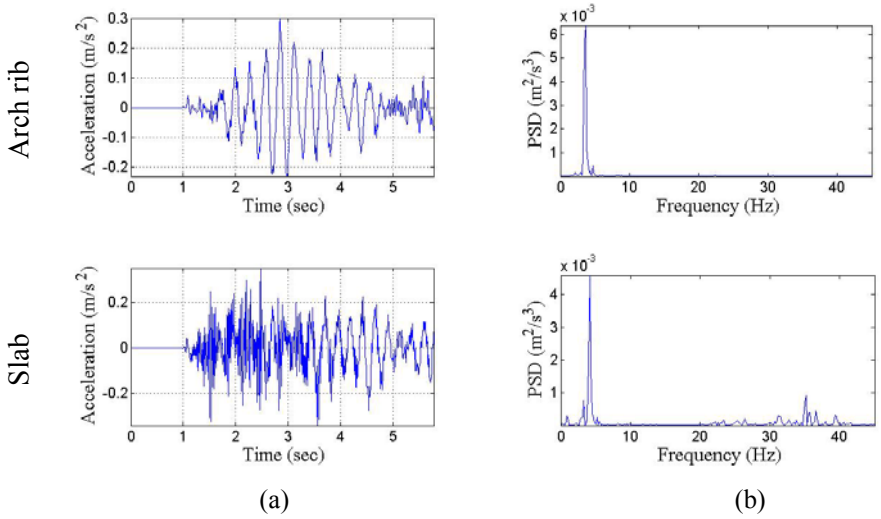

Figure 5 : Acceleration time history & power spectral density in middle span (Road surface profile=Perfect): (a)Time history of acceleration (b)Function of power spectral density

5 CONCLUSIONS

The study provides valuable information about the behaviour and dynamic response of the CFST tied-arch bridge. This information may be used to deduce DAFs for global and local vibrations. Based on the numerical result, the following conclusions can be drawn with respect to DAFs in a CFST tied-arch bridge:

(1) Modal Coupled Method is proved to be efficient for the analysis of the interaction between vehicle and CFST tied-arch bridge. With the method, the degree of freedom of the vehicle-bridge system can be remarkably reduced. Hence, the compution efficiency of the algorithm is improved. And stability and accuracy is ensured at the same time;

(2) Road surface profile of the bridge seriously affects the vehicle vibration, and thus the vehicle-bridge interaction. Since the condition of road surface in the future is difficult to be estimated precisely during the design stage, it is necessary to refine the specification of design codes for DAFs considering different road surface conditions. This can also be done by specifying a minimum requirement for road surface conditions to use the DAFs of the current code specification, especially for the maintenance and rating of existing bridges;

(3) Because the dynamic amplification factor is primarily used to amplify the internal static forces (axial force, moment, shear, etc.) in the design and evaluation of the bridge, it is therefore inappropriate to use the DAF calculated from the displacements. It is more logical to amplify the internal forces with local DAFs determined from the internal forces and reactions directly;

(4) Although the acceleration responses of arch ribs and hangers in time domain differ from each other, they have similar characteristics in frequency domain. The frequency response shows that the hangers vibrate mainly in their first mode. Shorter hangers are more susceptible to the vehicular impact than the longer ones.

REFERENCES

American association of state highway and transportation officials (AASHTO). 2005. LRFD Bridge Design Specifications. Washington (DC).

American association of state highway and transportation officials (AASHTO). 2004. Standard Specifications for Highway Bridges. Washington DC.

ANSYS, Inc. http://www.ansys.com.

Bhatt P. Programming the Dynamic Analysis of Structures. Spon Press, 11 New Fetter Lane, London EC4P 4EE.

Chen B.C. 2002. Examples of CFST Arch Bridges. Beijing: China Communications Press. (in Chinese)

Dodds C.J., Robson J.D. 1973. The description of road surface roughness. Journal of Sound and Vibration 31(2): p.175-183.

Fafard M, Laflamme M, Savard M, Bennur M. 1998. Dynamic analysis of existing continuous bridge. Journal of Bridge Engineering 3(1):p.28-37.

ISO. 1995. Mehcanical Vibration Road Surface Profiles Reporting of Measured Data. ISO 8608, IDT, Geneva.

Li Q., Tian X.M., Zhang Q.H. 2003. A model test on long-span x-style tied arch bridge on railway. China Railway Science 24(1): p.88-93. (in Chinese)

Lu J.G. 2005. Research on the damage of hangers of concrete-filled steel tubular arch bridges. Tianjin: Tianjin University. (in Chinese)

Malm R., Andersson A. 2006. Field testing and simulation of dynamic properties of a tied arch railway bridge. Engineering Structures 28, p.143–152.

Ontario Ministry of Transportation and Communication. 1983. Ontario Highway Bridge Design Code. Ontario.

Roeder C.W., MacRae G., Crocker P., Arima K., Wong Scott. 2000. Dynamic response and fatigue of steel tied-arch bridge. Journal of Brdige Engineering 5(1):p.14-21.

Shan D.S., Li Q. 2005. Coupled vibration analysis of x-style arch bridge and vehicles. Journal of Southwest Jiaotong University 40(1): p. 53-57. (in Chinese)

Trade Standard of People's Republic of China. 2004. JTG D60-2004 General Code for Design of Highway Bridges and Culverts. Beijing: China Comunications Press. (in Chinese)

Wu D.J., Wang X.S., Xiang H.F. 2003. The bridge-vehicle dynamics characteristic of Nelson arch bridge in high speed railway. Journal of the China Railway Society 25(3): p. 96-100. (in Chinese)